A thiocarbonate sink on the enzymatic energy landscape of aerobic CO oxidation? Answers from DFT and QM/MM models of Mo–Cu CO-dehydrogenases

Rovaletti, Anna; Bruschi, Maurizio; Moro, Giorgio; Cosentino, Ugo; Ryde, Ulf; Greco, Claudio

Published in:
Journal of Catalysis

DOI:
10.1016/j.jcat.2019.02.032

2019

Document Version:
Peer reviewed version (aka post-print)

A thiocarbonate sink on the enzymatic energy landscape of aerobic CO oxidation? Answers from DFT and QM/MM models of Mo–Cu CO-dehydrogenases

Anna Rovaletti,[a] Maurizio Bruschi,[a] Giorgio Moro,[b] Ugo Cosentino,[a] Ulf Ryde *[c] and Claudio Greco*[a]

We present a theoretical investigation providing key insights on a long-standing controversial issue that dominated the debate on carbon monoxide oxidation by Mo–Cu CO-dehydrogenases. Previous investigations gravitate around the possible occurrence of a thiocarbonate intermediate, that was repeatedly reported to behave as a thermodynamic sink on the catalytic energy landscape. By using a hierarchy of quantum mechanical and hybrid quantum/classical models of the enzyme, we show that no such energy sink is present on the catalytic energy profile. Consequent perspectives for the definition of a novel mechanistic proposal for the enzyme-catalyzed CO-oxidation are discussed in light of the recent literature.

1 Introduction

The MoCu-dependent CO-dehydrogenase (MoCu-CODH), expressed by the aerobic soil bacterium *Oligotropha carboxidovorans*, is an enzyme with key environmental relevance, as it detoxifies 2×10^8 tons of atmospheric CO annually [1]. Its catalytic mechanism has been the subject of extensive research efforts, which have led to controversies regarding the nature of the intermediates along the CO-oxidizing cycle giving rise to CO_2 evolution [2–5]. The MoCu-CODH active site presents a unique architecture in which the molybdenum ion shows a distorted square-pyramidal geometry (Fig. 1). An oxo (O^{2-}) ligand is found at the apex and the base is formed by a dithiolene ligand from a molybdopterin–cytosine dinucleotide (MCD) cofactor, another oxo ligand and a sulfido ligand. The latter bridges to the Cu ion, which is also coordinated by the sulfur atom of Cys388 and a weakly bound water molecule [6–8]. The copper ion remains in the +1 oxidation state throughout the catalytic cycle [2, 6]. Substrate binding and its oxidation are believed to occur at the Cu(I) center [9], owing to the high degree of delocalization within the Mo–S–Cu unit, allowing for facile electron transfer toward the redox-active Mo ion during catalysis [10].

The first mechanistic hypothesis for the catalytic cycle of MoCu-CODH was based on information coming from the crystal structure of the enzyme complexed with the *n*-butylisocyanide inhibitor [2]. According to this proposal, after CO binding to Cu(I), the equatorial oxo ligand of molybdenum (O_{eq}) may act as a nucleophile. Such a reaction would yield an intermediate with a five-membered ring, involving both the Mo and Cu ions. In the next step, CO may insert between the sulfido ligand and copper to yield a thiocarbonate intermediate (Fig. 1**D**), which is analogous to the thiocarbamate derivative formed during inhibition of the enzyme by *n*-butylisocyanide.

Inspired by this proposal, quantum mechanical (QM) studies based on density functional theory (DFT) were carried out on cluster models of the enzyme active site [3, 4]. These studies discovered an unexpected stability of the thiocarbonate intermediate which prevented an easy progress along the CO-oxidation mechanism. Siegbahn *et al.* suggested that the release of CO_2 can be facilitated by the binding of a water molecule to molybdenum. In another theoretical study, Hofmann and coworkers proposed that the thiocarbonate species is not part of the catalytic cycle. Based on their results, the thiocarbonate would represent a deep thermodynamic sink located outside the CO_2-evolving route, the presence of which would significantly slow down catalysis.

Both these QM studies were performed on small cluster models of the active site, which neglect most effects of the surrounding protein matrix. However, a more recent study showed that several residues surrounding the Mo–Cu binuclear center are crucial to maintain the structure of the enzyme core, arguing that a 179-atom QM model is needed for accurate results [8]. Unfortunately, this model has not yet been used to investigate the catalytic mechanism of the enzyme. Recently, the previously reported reaction mechanism for the oxidation of CO has been revisited by hybrid quantum mechanics/molecular mechanics (QM/MM) methods [11]. The study supported the formation of a relatively stable thiocarbonate adduct, lying somehow off-path the catalytic cycle. In fact, the authors suggested that the reaction has to follow a reverse process in order to release the CO_2 product from the thiocarbonate species.

By this study, we want to deepen the understanding of the controversial role of the thiocarbonate adduct in MoCu-CODH. We do so by using small and large-size QM cluster models of the active site, as well as QM/MM models of the whole enzyme. We show that the size of the model, as well as the level of theory, have a strong influence on the computed stability of the investigated intermediates. Most importantly, the thiocarbonate species turned out not represent a potential-energy well when the enzyme is described using large QM-cluster or all-atom QM/MM models, together with sufficiently large basis sets.

[a] *Deparment of Earth and Environmental Sciences, Milano – Bicocca University, Piazza della Scienza 1, 20126 Milan, Italy. E-mail: claudio.greco@unimib.it*

[b] *Department of Biotechnology and Biosciences, Milano – Bicocca University, Piazza della Scienza 2, 20126 Milan, Italy.*

[c] *Department of Theoretical Chemistry, Lund University, Chemical Centre, P.O. Box 124, SE-221 00 Lund, Sweden. E-mail: ulf.ryde@teokem.lu.se*

2 Computational Methods

All calculations were based on the crystal structure of the enzyme in its oxidized form (PDB ID: 1N5W) [2]. MoCu-CODH is a dimer of heterotrimers. In this study, only the large subunit of one dimer, containing the active site, was considered.

2.1 QM-cluster calculations (Models 1 & 2)

The smallest **Model 1** is the model used by Hofmann and coworkers and it is constituted by 24 atoms, representing the two metal centers and their first coordination sphere (shown in Fig. 2). **Model 2** is appreciably larger and it was created and validated by Rokhsana *et al.* [8]. It is composed of 179 atoms with CO substrate and 189 atoms when considering the *n*-butylisocyanide inhibitor. In addition to the atoms in **Model 1**, it includes also models of residues Gln240, Gly269–Gly272, Val384–Phe390, Tyr568–Ser570, and Glu763 (also shown in Fig. 2).

All QM calculations were carried out with DFT. Geometry optimizations were performed *in vacuo* using the TURBOMOLE 7.1 software with the BP86 method [12–14]. For **Model 1**, the calculations employed the def2-TZVP basis set, whereas for **Model 2**, the def2-TZVP basis set was used for the first coordination shell (31 or 41 atoms), whereas the rest of the model was described by the smaller def2-SVP basis set [12–15]. All calculations included Grimme's dispersion correction with Becke–Johnson damping (D3(BJ)) [16]. The resolution-of-identity technique was employed to accelerate the calculations [17]. For **Model 2**, all Cα atoms were kept frozen at the crystallographic positions together with one attached proton each. Finally, for both models, single-point energy calculations at the BP86 level were performed on the optimized geometries using the COSMO continuum solvent model [18], to evaluate solvation effects on the relative energies of the intermediates (ε=4). Moreover, the hybrid GGA functional B3LYP-D3(BJ) [19, 20], together with the large def2-TZVPD basis set, was employed to obtain more accurate energies.

2.2 QM/MM calculations (Model 3)

The QM/MM calculations required a detailed analysis of all protonable residues in the protein, based on calculations with PROPKA [21], studies of the hydrogen-bond pattern, the solvent accessibility and the possible formation of ionic pairs. Based on this analysis, we decided to let all Arg, Lys, Asp, and Glu residues be charged, with exception of Glu29 and Glu488 that were protonated on OE2, whereas Asp684 was protonated on OD1. Cysteine ligands coordinating to metals were deprotonated. Among the His residues, His61, 339, 766 and 793 were protonated on the ND1 atom, His177, 178, 210, 213, 243, 700, 753, 754 and 788 were assumed to be protonated on NE2 atom, whereas the other His residues were assumed to be doubly protonated. The protein was solvated with water molecules forming a sphere with a radius of 60 Å around the geometric center of the protein. Added protons and water molecules were then optimized by a 1-ns simulated-annealing molecular-dynamics simulation, followed by a minimization.

The QM/MM calculations were performed with the ComQum software [22, 23]. In this approach, the protein and the solvent are split into three subsystems: System 1 is the QM subsystem (containing 49 or 65 atoms considering CO or *n*-butylisocyanide, respectively, shown in the inset in Fig. 2 and in Figure S1 in the Supporting Information), System 2 consists of all residues with any atom within 6 Å of any atom in System 1, whereas System 3 contains the remaining part of the protein and the water molecules. During the QM/MM geometry optimizations, System 1 was relaxed by QM methods, whereas Systems 2 and 3 were kept fixed at the crystallographic coordinates. In the QM calculations, System 1 was represented by a wavefunction whereas all the other atoms were represented by an array of partial point charges.

Covalent bonds between the QM and MM systems were truncated using the hydrogen link-atom approach [24]. The QM system is capped with hydrogen atoms (hydrogen link atoms, HL), the position of which are linearly related to the corresponding carbon atoms (carbon link atoms, CL) in the full system [22]. The CL atoms are not included in the point-charge model. The total QM/MM energy in ComQum is calculated as

$$E_{\mathrm{QM/MM}} = E^{\mathrm{HL}}_{\mathrm{QM1+ptch23}} + E^{\mathrm{CL}}_{\mathrm{MM123},q_1=0} - E^{\mathrm{HL}}_{\mathrm{MM1},q_1=0} \qquad (1)$$

where $\mathrm{E}^{\mathrm{HL}}_{\mathrm{QM1+ptch23}}$ is the QM energy of System 1 truncated by HL atoms and embedded in the set of point charges modeling Systems 2 and 3. $\mathrm{E}^{\mathrm{HL}}_{\mathrm{MM1},q_1=0}$ is the MM energy of System 1, truncated by HL atoms, without any electrostatic interactions. $\mathrm{E}^{\mathrm{CL}}_{\mathrm{MM123},q_1=0}$ is the classical energy of the whole system, with CL atoms and with the charges present in System 1 set to zero, in order to avoid double counting of the electrostatic interactions. Thus, ComQum employs a subtractive scheme with electrostatic embedding and van der Waals link-atom corrections [25].

The QM calculations were carried out using TURBOMOLE 7.1 software [12]. Geometry optimizations were performed using the BP86 functional [13, 14] in combination with def2-TZVP basis set [15], including empirical dispersion correction D3(BJ) [16] and the resolution-of-identity technique to accelerate the calculations [17]. The MM calculations were carried out by means of the Amber software [26], using the Amber ff14SB force field for the protein [27], and the general Amber force field [28] with restrained electrostatic potential (RESP) charges [29] for carbon monoxide, *n*-butylisocyanide and MCD. The two Fe_2S_2 clusters were described with RESP charges and a non-bonded model (they are kept fixed in the calculations). Single-point calculations at B3LYP-D3(BJ)/def2-TZVPD [15, 19, 20] level were also run on the optimized geometries.

2.3 Big-QM calculation

More accurate QM/MM energies were also obtained by means of the Big-QM technique [30, 31]. This approach was developed to reduce the dependence of QM/MM energies on the size of the QM system and on the arbitrariness of the choice of the latter [32], based on the knowledge that QM/MM calculations converge faster than QM-only ones, but models of about 1000 QM atoms are needed to obtain convergence of the energies [33–36]. The minimal QM system (System 1) was extended with all chemical groups with at least one atom within 6.0 Å and junctions were moved two

amino-acids away from each residue in the minimal QM system. In addition, all buried charges inside the protein were included, with exception of the two iron–sulfur clusters (see Supporting Information Table S2). The resulting Big-QM model is constituted by 1060 atoms when the *n*-butylisocyanide ligand is present in the system. It is constituted by 990 atoms when the CO ligand is present instead (see Fig. 2). The Big-QM calculations were performed on coordinates from the QM/MM optimizations of **Model 3**, with a surrounding point-charge model, at the BP86-D3(BJ)/def2-SVP level. The multipole-accelerated resolution-of-identity *J* approach (marij keyword) was employed to accelerate the calculations [37]. The resulting energies were corrected with a QM/MM MM term (cf. Eqn. 1) for the Big-QM region:

$$E_{\mathrm{MM}} = E^{\mathrm{CL}}_{\mathrm{MM123},q_1=0} - E^{\mathrm{HL}}_{\mathrm{MM1},q_1=0} \tag{2}$$

Finally, the energies were also corrected by taking into consideration the B3LYP-D3(BJ)/def2-TZVPD functional and basis set effects, using calculations with the standard QM/MM QM system with a point-charge model of the surroundings:

$$E_{\mathrm{corr}} = E^{\mathrm{B3LYP/TZVPD}}_{\mathrm{QM1,ptch23}} - E^{\mathrm{BP86/SVP}}_{\mathrm{QM1,ptch23}} \tag{3}$$

3 Results

In this work, we focus on the first steps of the CO-oxidation mechanism and on the associated side reaction described by Hofmann and coworkers [4]. In particular, we consider the thiocarbonate adduct (**D** in Fig. 1) and the intermediates that give rise to it (**A**, **B** and **C** in Fig. 1).

Structural comparison of each of these species, optimized using models **1**–**3**, showed great structural similarity (see Supporting Information, Table **S3**). The mean absolute deviation for the bonded distances in this table between **Model 1** or **Model 2** and **Model 3** is only 0.03 and 0.02 Å, respectively. The maximum deviation is 0.10 Å, observed both for the Cu–C(CO) bond in intermediate **A** and for the Mo–O_{eq} bond in intermediate **D** for **Model 1**.

Larger differences are observed when comparing distances between non-bonded atoms. In particular, the position of the CO substrate with respect to the putative nucleophile O_{eq} in **A** depends strongly on the model size. As the description of the active site environment becomes more and more complete, the C $\cdots$ O_{eq} distance becomes considerably shorter (3.54, 2.62 and 2.26 Å for **Models 1**, **2** and **3**, respectively). The latter result suggests that the protein surrounding the active site has a role to assist the correct positioning of the substrate with respect to the incipient nucleophile. The presence of the aromatic ring of Phe390 in front of the Cu ion might be responsible of this effect, as it was proposed to influence the nature of the interaction between the copper ion and a weakly-coordinated water molecule in the crystallographic experiments [8].

Moreover, mutation of Phe390 to Tyr was reported to partially impair CO-oxidation catalysis [38]. The latter experimental evidence further illustrates the importance of going beyond the first coordination sphere when details on CO binding and processing need to be modeled. In this regard, it is interesting to notice that a variant of **Models 1** supplemented simply with the inclusion of the sidechain of residue 390 gives place to unreliable structures already at the level of the substrate-unbound form of the enzyme (see Figure SX in SI)

The relevance of the second coordination sphere and of the long-range effects of the protein matrix becomes evident also when the relative energies of the various intermediates are considered (see Table 1). We focus first on the stability of **D**, given the key relevance of this thiocarbonate intermediate in previous theoretical investigations of MoCu-CODH. The computed ΔE_{DA} between **D** and the parent adduct **A** is large in the case of **Model 1**, which is not surprising given the results of previous studies based on small models of the active site ($\Delta E^{\mathrm{Model1}}_{\mathrm{DA}}$ = –47 kJ/mol). However, the energy difference becomes much smaller when the size of the model increases: $\Delta E^{\mathrm{Model2}}_{\mathrm{DA}}$ = –25 kJ/mol, $\Delta E^{\mathrm{Model3}}_{\mathrm{DA}}$ = –8 kJ/mol. The latter energy difference shrinks further when Big-QM/MM corrections are adopted ($\Delta E^{\mathrm{BigQM}}_{\mathrm{DA}}$ = –5 kJ/mol).

As for intermediate **B**, the ΔE_{BA} energy differences appear to depend much less on the size of the adopted model, with a variation of up to 23 kJ/mol. More specifically, ΔE_{BA} is essentially independent of the second coordination sphere (Models **1** and **2** give nearly identical energies), whereas inclusion of long-range interactions influences the energy difference somewhat more (cf. the QM/MM results in Table 1).

The effect of the second coordination sphere of the metals turned out to be more pronounced when the stability of intermediate **C** is considered. In fact, for **Model 1**, this intermediate is predicted to be very stable ($\Delta E^{\mathrm{Model1}}_{\mathrm{CA}}$ = –60 kJ/mol). However, the computed energy difference becomes much smaller when the active site model includes the second coordination sphere ($\Delta E^{\mathrm{Model2}}_{\mathrm{CA}}$ = –22 kJ/mol), and it shrinks further when the whole protein is considered (ΔE_{CA} = –2 kJ/mol and –12 kJ/mol in the case of QM/MM calculations without or with Big-QM corrections, respectively).

In analogy with some of the previous studies on the catalytic mechanism of the MoCu-CODH [4, 11], we also carried out ancillary calculation on the inhibition of the enzyme by *n*-butylisocyanide (|C≡N–R, a ligand that is isoelectronic with the |C≡O substrate). This was done to assess the capability of our larger models to reproduce the deep potential well associated with the formation of a thiocarbamate adduct, which is at the basis of the experimentally observed inhibition. Analogously to previous reports, the stability of the thiocarbamate adduct (**F** in Fig. 1) was evaluated by considering the parent encounter complex as a reference (**E** in Fig. 1). As expected, our calculations show for all four models a high stability of the thiocarbamate product **F** with respect to the reference **E**: ΔE_{FE} = –66 to –97 kJ/mol, as can be seen in Table 2. Thus, our large-sized models – and in particular the Big-QM calculations – provide energy landscapes that are compatible both with the inhibitory role of the thiocarbamate adduct and with a non-inhibitory role of the thiocarbonate intermediate.

4 Discussion

In this work, we evaluated the relative stability of the thiocarbonate intermediate in MoCu-CODH, whose formation is thought to represent a key intermediate during catalytic CO oxidation. To this end, a hierarchy of QM-cluster models of different sizes, as well as

QM/MM models were adopted to describe the enzyme.

Our results from a small QM-cluster model including only the metal ions and their first coordination sphere suggest that the thiocarbonate adduct corresponds to a deep well on the potential-energy surface. Notably, the early studies by Hofmann, Siegbahn, and coworkers [3, 4], reported energies even more negative for this intermediate (up to –93 kJ/mol as compared to the encounter complex). The latter models not only bear the shortcomings from complete or partial neglect of the second coordination sphere. In fact, the lack of dispersion energy corrections in those studies was later reported to contribute to inaccuracies in the calculation of energy differences involving the thiocarbonate intermediate [39]. In a recent QM/MM study by Xu and Hirao, the thiocarbonate conformer was predicted to be less stable. However, according to those authors, this species would still represent a thermodynamic sink, with a QM/MM ΔE_{DA} energy difference of –43 kJ/mol. This would drive the enzyme somehow off-path when the **C** intermediate is reached, as the rearrangement of the latter to give the thiocarbonate adduct was reported to be energetically favorable. Notably, the basis set used in the latter QM/MM study for geometry optimizations was of double-zeta quality both for metal atoms and for light atoms. Previous studies on similar Mo-containing systems have suggested that the choice of the basis set is critical to obtain accurate energies [40, 41]. An evaluation of the influence of the quality of the basis set used during the optimization on our system, evidenced an effect of 19 kJ/mol on the final energies even when the involved intermediates retain a high degree of structural similarity (see Supporting Information, Tables S4 and S5).

In conclusion, accurate modeling of the protein surroundings around the active site, coupled with consideration of dispersion effects and employment of sufficiently large basis sets allowed us to reveal that the thiocarbonate adduct does not play the role of an unusual rate-limiting intermediate in MoCu-CODH. Instead, our results are in line with a recent proposal [9] that intermediates **B**, **C** and **D** may be readily interconverted during biocatalysis.

Table 1 Relative energies (kJ/mol) of the intermediates **A**, **B**, **C** and **D**, calculated using the QM-cluster models, the QM/MM model and the Big-QM approach at B3LYP-D3(BJ)/def2-TZVPD level.

	A	B	C	D
Model 1	0.0	-5.0	-60.2	-46.9
Model 2	0.0	-2.1	-21.8	-25.1
Model 3	0.0	-24.7	-2.1	-8.4
Big-QM	0.0	-15.5	-11.7	-5.0

Table 2 Relative energies (kJ/mol) of the intermediates **E** and **F**, calculated using the QM-cluster models, the QM/MM model and the Big-QM approach at B3LYP-D3(BJ)/def2-TZVPD level.

	E	F
Model 1	0.0	-89.9
Model 2	0.0	-88.3
Model 3	0.0	-97.1
Big-QM	0.0	-65.7

References

1 G. Mörsdorf, K. Frunzke, D. Gadkari, and O. Meyer, "Microbial growth on carbon monoxide," *Biodegradation*, vol. 3, no. 1, pp. 61–82, 1992.

2 H. Dobbek, L. Gremer, R. Kiefersauer, R. Huber, and O. Meyer, "Catalysis at a dinuclear [CuSMo (O) OH] cluster in a CO dehydrogenase resolved at 1.1-Å resolution," *PNAS*, vol. 99, no. 25, pp. 15971–15976, 2002.

3 P. E. Siegbahn and A. F. Shestakov, "Quantum chemical modeling of CO oxidation by the active site of molybdenum CO dehydrogenase," *J Comput Chem*, vol. 26, no. 9, pp. 888–898, 2005.

4 M. Hofmann, J. K. Kassube, and T. Graf, "The mechanism of Mo-/Cu-dependent CO dehydrogenase," *JBIC*, vol. 10, no. 5, pp. 490–495, 2005.

5 R. Hille, S. Dingwall, and J. Wilcoxen, "The aerobic CO dehydrogenase from Oligotropha carboxidovorans," *JBIC*, vol. 20, no. 2, pp. 243–251, 2015.

6 M. Gnida, R. Ferner, L. Gremer, O. Meyer, and W. Meyer-Klaucke, "A novel binuclear [CuSMo] cluster at the active site of carbon monoxide dehydrogenase: characterization by X-ray absorption spectroscopy," *Biochemistry*, vol. 42, no. 1, pp. 222–230, 2003.

7 J. Wilcoxen and R. Hille, "The Hydrogenase Activity of the Molybdenum/Copper-containing Carbon Monoxide Dehydrogenase of Oligotropha carboxidovorans," *J Biol Chem*, vol. 288, no. 50, pp. 36052–36060, 2013.

8 D. Rokhsana, T. A. Large, M. C. Dienst, M. Retegan, and F. Neese, "A realistic in silico model for structure/function studies of molybdenum–copper CO dehydrogenase," *JBIC*, vol. 21, no. 4, pp. 491–499, 2016.

9 M. Shanmugam, J. Wilcoxen, D. Habel-Rodriguez, G. E. Cutsail III, M. L. Kirk, B. M. Hoffman, and R. Hille, "13C and 63, 65Cu ENDOR studies of CO Dehydrogenase from Oligotropha carboxidovorans. Experimental Evidence in Support of a Copper–Carbonyl Intermediate," *JACS*, vol. 135, no. 47, pp. 17775–17782, 2013.

10 C. Gourlay, D. J. Nielsen, J. M. White, S. Z. Knottenbelt, M. L. Kirk, and C. G. Young, "Paramagnetic active site models for the molybdenum-copper carbon monoxide dehydrogenase," *JACS*, vol. 128, no. 7, pp. 2164–2165, 2006.

11 K. Xu and H. Hirao, "Revisiting the catalytic mechanism of Mo–Cu carbon monoxide dehydrogenase using QM/MM and DFT calculations," *Phys Chem Chem Phys*, vol. 20, no. 28, pp. 18938–18948, 2018.

12 "TURBOMOLE V7.1 2016, a development of University of Karlsruhe and Forschungszentrum Karlsruhe GmbH, 1989-2007, TURBOMOLE GmbH, since 2007; available from `http://www.turbomole.com`.."

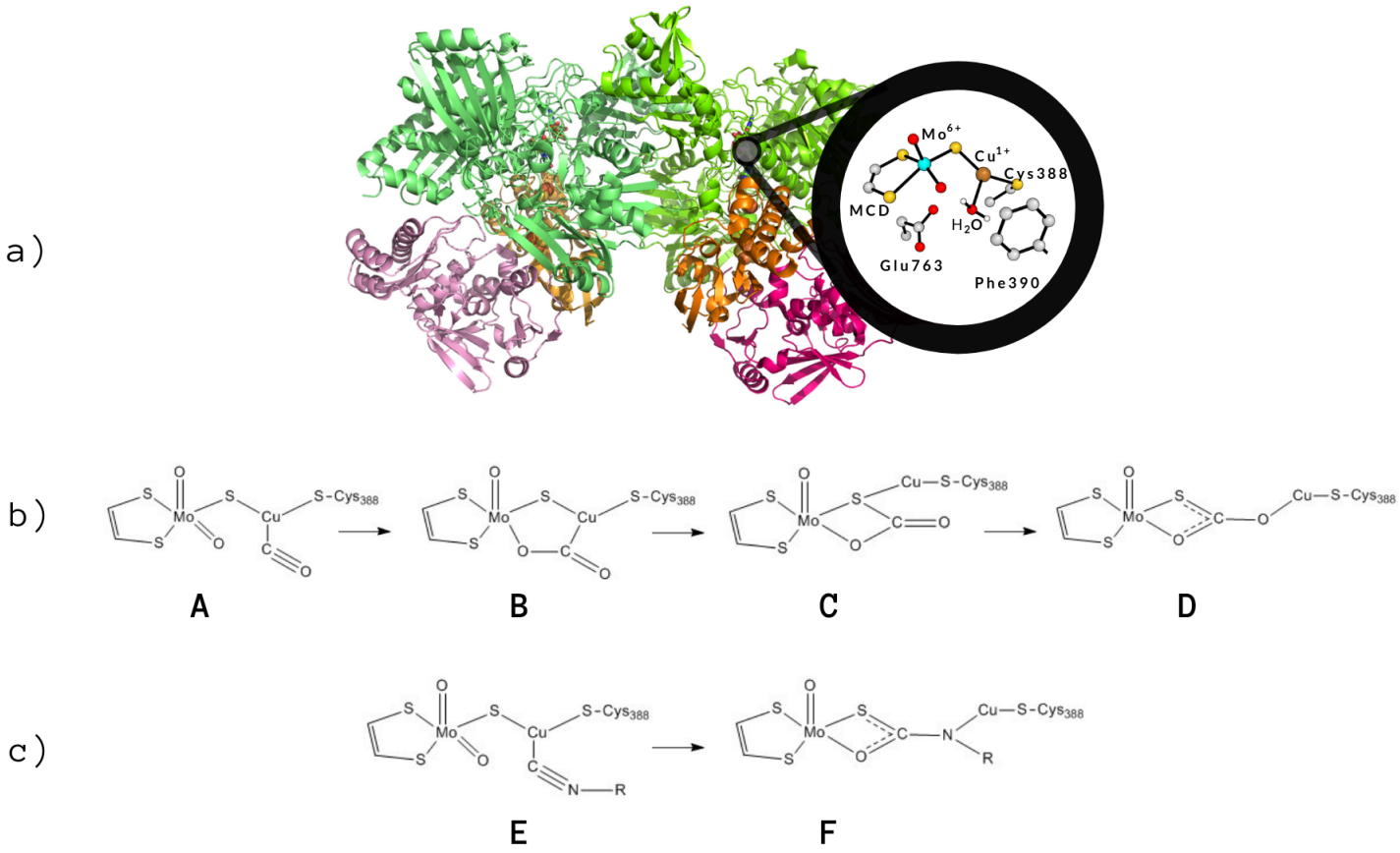

Fig. 1 (a) Representation of the MoCu-CODH enzyme and of the active site in the Mo(VI)Cu(I) resting state; (b) Intermediates involved in the thiocarbonate-formation mechanism; (c) Intermediates involved during inhibition of MoCu-CODH by *n*-butylisocyanide. R = *n*-butyl.

13 A. D. Becke, "Density-functional exchange-energy approximation with correct asymptotic behavior," *Phys Rev A*, vol. 38, no. 6, p. 3098, 1988.

14 J. P. Perdew, "Density-functional approximation for the correlation energy of the inhomogeneous electron gas," *Phys Rev B*, vol. 33, no. 12, p. 8822, 1986.

15 F. Weigend and R. Ahlrichs, "Balanced basis sets of split valence, triple zeta valence and quadruple zeta valence quality for H to Rn: Design and assessment of accuracy," *Phys Chem Chem Phys*, vol. 7, no. 18, pp. 3297–3305, 2005.

16 S. Grimme, S. Ehrlich, and L. Goerigk, "Effect of the damping function in dispersion corrected density functional theory," *J Comput Chem*, vol. 32, no. 7, pp. 1456–1465, 2011.

17 K. Eichkorn, F. Weigend, O. Treutler, and R. Ahlrichs, "Auxiliary basis sets for main row atoms and transition metals and their use to approximate Coulomb potentials," *Theo Chem Acc*, vol. 97, no. 1, pp. 119–124, 1997.

18 A. Klamt and G. Schüürmann, "COSMO: a new approach to dielectric screening in solvents with explicit expressions for the screening energy and its gradient," *J Chem Soc*, no. 5, pp. 799–805, 1993.

19 A. D. Becke, "A new mixing of Hartree–Fock and local density-functional theories," *J Phys Chem*, vol. 98, no. 2, pp. 1372–1377, 1993.

20 C. Lee, W. Yang, and R. G. Parr, "Development of the Colle-Salvetti correlation-energy formula into a functional of the electron density," *Phys Rev B*, vol. 37, no. 2, p. 785, 1988.

21 M. H. Olsson, C. R. Søndergaard, M. Rostkowski, and J. H. Jensen, "PROPKA3: consistent treatment of internal and surface residues in empirical pKa predictions," *J Chem Theory Comput*, vol. 7, no. 2, pp. 525–537, 2011.

22 U. Ryde, "The coordination of the catalytic zinc ion in alcohol dehydrogenase studied by combined quantum chemical and molecular mechanical calculations," *J Comput Aid Mol Des*, vol. 10, pp. 153–164, 1996.

23 U. Ryde and M. H. Olsson, "Structure, strain, and reorganization energy of blue copper models in the protein," *Int J Quantum Chem*, vol. 81, no. 5, pp. 335–347, 2001.

24 N. Reuter, A. Dejaegere, B. Maigret, and M. Karplus, "Frontier bonds in QM/MM methods: A comparison of different approaches," *J Phys Chem A*, vol. 104, no. 8, pp. 1720–1735, 2000.

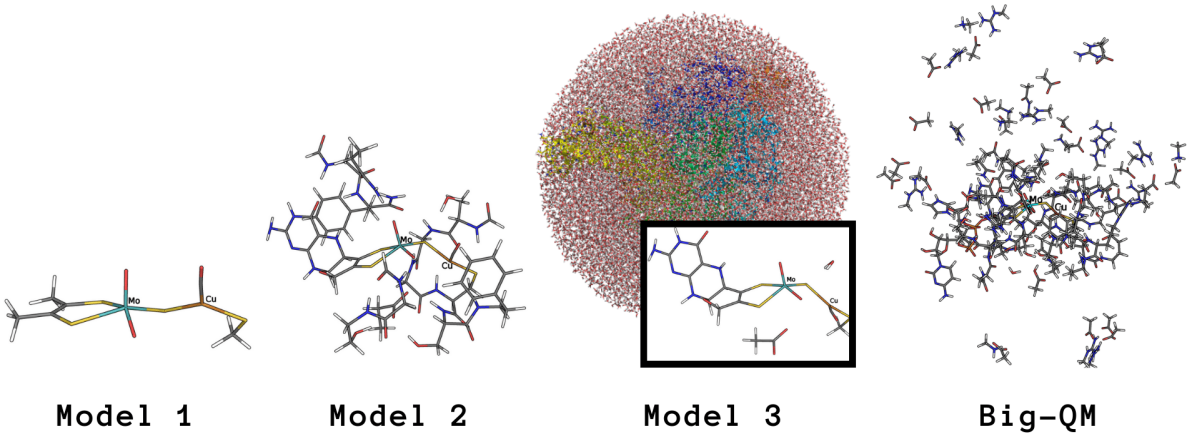

Fig. 2 Models used for the description of the MoCu-dependent CO-dehydrogenase. Color code of atoms: cyan, molybdenum; brown, copper; yellow, sulphur; red, oxygen; grey, carbon; white, hydrogen.

25 L. Cao and U. Ryde, "On the difference between additive and subtractive QM/MM calculations," *Frontiers in chemistry*, vol. 6, p. 89, 2018.

26 D. Case, V. Babin, J. Berryman, R. Betz, Q. Cai, D. Cerutti, T. Cheatham Iii, T. Darden, R. Duke, H. Gohlke, *et al.*, "Amber 14," 2014.

27 J. A. Maier, C. Martinez, K. Kasavajhala, L. Wickstrom, K. E. Hauser, and C. Simmerling, "ff14SB: improving the accuracy of protein side chain and backbone parameters from ff99SB," *J Chem Theory Comput*, vol. 11, no. 8, pp. 3696–3713, 2015.

28 J. Wang, R. M. Wolf, J. W. Caldwell, P. A. Kollman, and C. D. A., "Development and testing of a general amber force field," *J. Comput. Chem.*, vol. 25, pp. 1157–1174, 2004.

29 C. I. Bayly, P. Cieplak, W. D. Cornell, and P. A. Kollman, "A well-behaved electrostatic potential based method using charge restraints for deriving atomic charges: The resp model," *J. Phys. Chem.*, vol. 97, pp. 10269–10280, 1993.

30 L. Hu, P. Söderhjelm, and U. Ryde, "Accurate reaction energies in proteins obtained by combining QM/MM and large QM calculations," *J Chem Theory Comput*, vol. 9, no. 1, pp. 640–649, 2012.

31 S. Sumner, P. Söderhjelm, and U. Ryde, "Effect of geometry optimizations on QM-cluster and QM/MM studies of reaction energies in proteins," *J Chem Theory Comput*, vol. 9, no. 9, pp. 4205–4214, 2013.

32 L. Hu, J. Eliasson, J. Heimdal, and U. Ryde, "Do quantum mechanical energies calculated for small models of protein-active sites converge?," *J Phys Chem A*, vol. 113, no. 43, pp. 11793–11800, 2009.

33 C. V. Sumowski and C. Ochsenfeld, "A convergence study of QM/MM isomerization energies with the selected size of the QM region for peptidic systems," *The Journal of Physical Chemistry A*, vol. 113, no. 43, pp. 11734–11741, 2009.

34 D. Flaig, M. Beer, and C. Ochsenfeld, "Convergence of electronic structure with the size of the QM region: example of QM/MM NMR shieldings," *Journal of chemical theory and computation*, vol. 8, no. 7, pp. 2260–2271, 2012.

35 R.-Z. Liao and W. Thiel, "Convergence in the QM-only and QM/MM modeling of enzymatic reactions: A case study for acetylene hydratase," *Journal of computational chemistry*, vol. 34, no. 27, pp. 2389–2397, 2013.

36 S. Roßbach and C. Ochsenfeld, "Influence of coupling and embedding schemes on QM size convergence in QM/MM approaches for the example of a proton transfer in DNA," *Journal of chemical theory and computation*, vol. 13, no. 3, pp. 1102–1107, 2017.

37 M. Sierka, A. Hogekamp, and R. Ahlrichs, "Fast evaluation of the Coulomb potential for electron densities using multipole accelerated resolution of identity approximation," *J Chem Phys*, vol. 118, no. 20, pp. 9136–9148, 2003.

38 P. Kaufmann, B. R. Duffus, C. Teutloff, and S. Leimkühler, "Functional studies on oligotropha carboxidovorans molybdenum–copper CO dehydrogenase produced in Escherichia coli," *Biochemistry*, vol. 57, no. 19, pp. 2889–2901, 2018.

39 P. E. Siegbahn, "The effect of backbone constraints: the case of water oxidation by the oxygen-evolving complex in PSII," *Chem Phys Chem*, vol. 12, no. 17, pp. 3274–3280, 2011.

40 J.-L. Li, R. A. Mata, and U. Ryde, "Large density-functional and basis-set effects for the DMSO reductase catalyzed oxo-transfer reaction," *J Chem Theory Comput*, vol. 9, no. 3, pp. 1799–1807, 2013.

41 J. Li, M. Andrejić, R. A. Mata, and U. Ryde, "A computational comparison of oxygen atom transfer catalyzed by dimethyl sulfoxide reductase with Mo and W," *Eur J Inorg Chem*, vol. 2015, no. 21, pp. 3580–3589, 2015.